Wavelet-Based Adaptive Grid Method for the Resolution of Nonlinear PDEs

Paulo Cruz, Adélio Mendes, and Fernão D. Magalhães
LEPAE-Chemical Engineering Dept., Faculty of Engineering, University of Porto, 4200-465 Porto, Portugal

Theoretical modeling of dynamic processes in chemical engineering often implies the numeric solution of one or more partial differential equations. The complexity of such problems is increased when the solutions exhibit sharp moving fronts. A new numerical method is established, based on interpolating wavelets, that dynamically adapts the collocation grid so that higher resolution is automatically attributed to domain regions where sharp features are present. The effectiveness of the method is demonstrated with some relevant examples in a chemical engineering context.

Introduction

The mass- and heat-transport phenomena present in the conventional processes involving separation, reaction, and fluid transport are usually described through one or several partial differential equations (PDEs). The mathematical simulation of such processes, for design or optimization purposes, necessarily implies the solution of those equations. It is therefore important to have efficient and accurate tools for solving PDEs when performing theoretical modeling in chemical engineering.

The numerical methods are usually applied to this type of problem can be divided into two groups: finite differences methods (FDM) and weight residual methods (WRM) (Finlayson, 1992). The latter differ from each other in terms of the weighing functions chosen. The most common are collocation method, Galerkin method, and least-square method (Finlayson, 1980).

If the PDE solution is regular, any of these methods can be applied with success. However, singularities and abrupt transitions are associated with many phenomena, such as concentration and or temperature fronts in fixed-bed processes, temperature "hot-spot" in continuous reactors, and shock waves in the flow of compressive gases or in polymer flow. This implies the use of adaptive methods: adaptive finite differences or moving finite elements (Sereno, 1989). The largest difficulty with such methods is determining the mobility of the grid or the finite elements (usually based on empiric expressions) and the accurate definition of the function when a new grid point or element is added between two existing grid points or elements.

Wavelets are a relatively new mathematical concept, introduced at the end of the 1980s (Daubechies, 1988, 1992; Mallat, 1989); for a brief introduction, see DeVore and Lucier (1992), Graps (1995), Jawerth and Sweldens (1994), and Strang (1989, 1994). The term "wavelet" is used in general to describe a function that features compact support. This means that the function is located spatially, only being different from zero in a finite interval.

The great advantage of this type of function, compared to the conventional functions used in data representation, is that different resolution levels can be used to describe distinct space or time regions. This feature is quite useful in signal, sound, and image compression algorithms. When a data set goes through a wavelet transformation, it is decomposed into two types of coefficients: one represents general features (scaling function coefficients) and another describes localized features (wavelet coefficients). In order to perform data compression, the wavelet coefficients corresponding to regions in space of less importance are partially rejected. Then, when the function is reconstructed, high resolution is maintained only in the relevant regions. This localized resolution feature does not exist in plane waves, which have constant resolution throughout the entire domain.

Several articles have been published recently in the fields of applied mathematics and physics that present wavelet-based methods for resolution of PDEs. These are classified as collocation methods (Bertoluzza, 1996, 1997; Cai and

Correspondence concerning this article should be addressed to F. D. Magalhães.

Wang, 1996; Holmström, 1999; Jameson, 1994, 1998; Kaibara and Gomes, 2001; Vasilyev and Paolucci, 1996, 1997; Waldén, 1999) or Galerkin methods (Bacry et al., 1992; Beylkin and Keiser, 1997; Charton and Perrier, 1996; Dahmen et al., 1996; Fröhlich and Shneider, 1997; Griebel and Koster, 2000; Holmström and Waldén, 1998; Lazaar et al., 1994; Liandrat and Tchamitchian, 1990; Monasse and Perrier, 1998; Restrepo and Leaf, 1995). The two methods differ in that Galerkin methods obtain the solution in the wavelet coefficient space and in general can be considered gridless methods. In the collocation methods, on the other hand, the solution is obtained in the physical space over a dynamically adapted grid. Each wavelet is univocally associated with a collocation point and the grid adaptation is based on the analysis of the wavelet coefficients. For a certain integration time, the grid consists of those points that correspond to wavelet coefficients whose value is above a predefined threshold (a parameter that controls the accuracy of the solution).

In a recent article, Cruz et al. (2001) established a collocation method that combines different approaches found in previous works, emphasizing the advantages of wavelet-based methods over conventional ones. The present work intends to extend that technique to the solution of PDEs with nonlinear coefficients and to the solution of systems of PDEs.

Key Concepts and Definitions

The present description is not concerned with extended mathematical derivations, but only with the more important definitions and concepts, in order to keep a pragmatic engineering perspective. A more detailed mathematical treatment can be found in, for instance, Daubechies (1992).

The term wavelet is used to describe a function with compact support. This means the function is located in space, that is, the function is only different from zero in a finite region of the domain. The wavelet families that have been proposed in the mathematical literature can be classified as orthogonal or biorthogonal. A brief description is presented next.

Orthogonal family

Two functions, the mother scaling function, ϕ, and the mother wavelet, ψ, characterize each orthogonal family. These are defined by the following recursive relations

$$\phi(x)=\sqrt{2}\sum_{j=-m}^{m} h_j\phi(2x-j),\ \psi(x)=\sqrt{2}\sum_{j=-m}^{m} g_j\phi(2x-j) \tag{1}$$

where h_j and g_j are the filters that characterize the family of degree m. These filters must satisfy orthogonality and symmetry relations (Jameson, 1994).

Due to the choice of the filters h_j and g_j, the dilations and translations of the mother scaling function, $\phi_k^j(x)$, and the mother wavelet, $\psi_k^j(x)$, form an orthogonal basis of $\mathbf{L}^2(\mathbb{R})$ (Jameson, 1994). This property has an important consequence: any continuous function $f(x)$ can be uniquely projected in this orthogonal basis and expressed as, for example, a linear combination of functions $\psi_k^j(x)$

$$f(x)=\sum_{j\in\mathbb{Z}}\sum_{k\in\mathbb{Z}} d_k^j\psi_k^j(x) \tag{2}$$

where

$$d_k^j=\int_{-\infty}^{\infty} f(x)\psi_k^j(x)dx$$

Biorthogonal family

Four functions: the mother scaling function ϕ, the mother wavelet ψ, the dual scaling function $\tilde{\phi}$, and the dual wavelet $\tilde{\psi}$, define each biorthogonal family. These are defined by the following recursive relations

$$\phi(x)=\sum_{j=-m}^{m} h_j\phi(2x-j),\ \psi(x)=\sum_{j=-m}^{m} g_j\phi(2x-j) \tag{3}$$

$$\tilde{\phi}(x)=2\sum_{j=-m}^{m} \tilde{h}_j\tilde{\phi}(2x-j),\ \tilde{\psi}(x)=2\sum_{j=-m}^{m} \tilde{g}_j\tilde{\phi}(2x-j) \tag{4}$$

where h_j, $\tilde{h}_j$, g_j, and $\tilde{g}_j$ are the filters that characterize the family of degree m. These filters must satisfy orthogonality and symmetry relations (Waldén, 1999).

Some graphical examples of orthogonal and biorthogonal wavelet families can be found in Shi et al. (1999).

Multiresolution Analysis

The multiresolution analysis consists of a sequence of two closed subspaces, V^j, $\tilde{V}^j$, belonging to $\mathbf{L}^2(\mathbb{R})$, that satisfy

$$\cdots\subset V^{-2}\subset V^{-1}\subset V^0\subset V^1\subset V^2\subset\cdots$$

$$\cdots\subset \tilde{V}^{-2}\subset \tilde{V}^{-1}\subset \tilde{V}^0\subset \tilde{V}^1\subset \tilde{V}^2\subset\cdots$$

where V^j is a space of scaling functions and $\tilde{V}^j$ is a space of the corresponding dual scaling functions, and j represents the resolution level:

- If a function $f(x)$ is contained in the space V^j, the function $f(2x)$ must be contained in a space of higher resolution, V^{j+1}: $f(x)\in V^j \Leftrightarrow f(2x)\in V^{j+1}$; $f(x)\in \tilde{V}^j \Leftrightarrow f(2x)\in \tilde{V}^{j+1}$.
- If a function is contained in the space V^j, its integer translation has to be contained in the same space V^j: $f(x)\in V^j \Leftrightarrow f(x+k)\in V^j$; $f(x)\in \tilde{V}^j$, $\Leftrightarrow f(x+k)\in V^j$, $j,\ k\in\mathbb{Z}$.
- The union of all spaces V^j is the space $\mathbf{L}^2(\mathbb{R})$: $\overline{\cup_k V^j}=\overline{\cup_k \tilde{V}^j}=\mathbf{L}^2(\mathbb{R})$, $j\in\mathbb{Z}$.
- The interception of all spaces V^j is the element 0: $\cap_k V^j=\cap_k \tilde{V}^j=\{0\}$.
- The wavelets spaces W^j and $\tilde{W}^j$ are defined as orthogonal spaces and are complementary of V^j in V^{j+1}, $V^{j+1}=V^j\oplus W^j$, $\tilde{V}^{j+1}=\tilde{V}^j\oplus\tilde{W}^j$.

Expansion of a Continuous Function

The expansion of a continuous function in wavelet theory can be performed according to two representations. The first scaling function representation involves only the scaling functions; the second, wavelet representation, involves both wavelets and scaling functions. The representations are equivalent and need the exact same number of coefficients. One can move from one representation to the other by using a process designated as *wavelet transform* (Waldén, 1999). The scaling function representation is given by

$$f(x) = \sum_k s_k^{J\max} \phi_k^{J\max}(x) \tag{5}$$

where

$$s_k^{J\max} = \int \tilde{\phi}_k^{J\max}(x) f(x)\, dx$$

where s are the scaling function coefficients, $J_{\max}$ is the maximum resolution level, and k represents the spatial location. The wavelet representation is given by

$$f(x) = \sum_{k \in \mathbb{Z}} s_k^{J\min} \phi_k^{J\min}(x) + \sum_{j \in \mathbb{Z}} \sum_{k \in \mathbb{Z}} d_k^j \psi_k^j(x) \tag{6}$$

where d are the wavelet coefficients and $J_{\min}$ the minimum resolution level

$$d_k^j = \int_{-\infty}^{\infty} f(x) \tilde{\psi}_k^j(x)\, dx \text{ and } s_k^{J\min} = \int_{-\infty}^{\infty} f(x) \tilde{\phi}_k^j(x)\, dx \tag{7}$$

Integrations have to be performed in order to compute the expansion coefficients. Several methods have been proposed in the literature for accomplishing this, starting from a function's discrete values. These methods necessarily introduce a certain approximation error and increase the complexity of the problem, namely in the solution of PDEs. There is, however, a wavelet family for which these integrations are exact: the interpolating wavelets. This wavelet family has been given different names in the most recent literature: Daubechies autocorrelation function (Saito and Beylkin, 1993), interpolating Lagrange wavelets (Shi et al., 1999), or Deslaurier–Dubuc function (Deslaurier and Dubuc, 1989). This family is described in detail below.

Interpolating Wavelets

The interpolating wavelet is related to the construction of a continuous function $\phi(x)$, when only a finite number of function values, ϕ_i, are known (Deslaurier and Dubuc, 1989), where

$$\phi_i = \begin{cases} 1 & \text{if} \quad i = 0 \\ 0 & \text{if} \quad i \neq 0, \end{cases} \quad i \in \mathbb{Z} \tag{8}$$

One way of building this function is by recursive interpolation in a dyadic grid, $V^j = \{x_k^j \in \mathbb{R}:\ x_k^j = k/2^j,\ k \in \mathbb{Z}\}\ j \in \mathbb{Z}$, where x_k^j are the grid points, j identifies the resolution level, and k the spatial location (Figure 1). Since $x_k^{j-1} = x_{2k}^j$, the key multiresolution condition is verified: $V^{j-1} \subset V^j$.

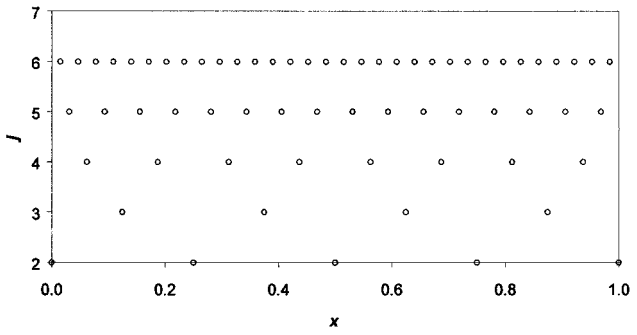

Figure 1. Example of collocation points in a dyadic grid.

The filters h and $\tilde{h}$ for this wavelet family are, respectively, $h_j = \phi(j/2)$ and $\tilde{h}_j = \delta_j$, $j = -m+1,\ m-1$. The two remaining filters can be calculated through the symmetry relations (Waldén, 1999), therefore completely specifying this wavelet family. This way the evaluation of the convolution integrals for computing the wavelet coefficients and scaling function coefficients, Eqs. 5 to 7, can be evaluated exactly using a single value (scaling function coefficients) or using a few values (wavelet coefficients).

For this special wavelet family, the determination of the scaling function coefficients and the wavelet coefficients can be made using an alternative approach, more intuitive, based on multiresolution analysis. If a function, $f^j(x)$, belongs to space V^j, then the function f^{j+1} belongs to space V^{j+1}. Due to the wavelet interpolating property, it is verified that $f^j(x_k^j) = f(x_k^j)$ and, because $x_k^j = x_{2k}^{j+1}$, then $f^j(x_{2k}^{j+1}) = f^{j+1}(x_{2k}^{j+1})$. However, $f^j(x_{2k+1}^{j+1}) \neq f^{j+1}(x_{2k+1}^{j+1})$. This way, the wavelet coefficients can be calculated easily from Eq. 9 (see Figure 2)

$$d_k^j = f^{j+1}\left(x_{2k+1}^{j+1}\right) - f^j\left(x_{2k+1}^{j+1}\right),\ f^j\left(x_k^j\right) = f^{j+1}\left(x_{2k}^{j+1}\right) \tag{9}$$

All the necessary concepts for a function representation in a wavelet basis have been presented. Next we describe some aspects of a more specific implementation in terms of PDE

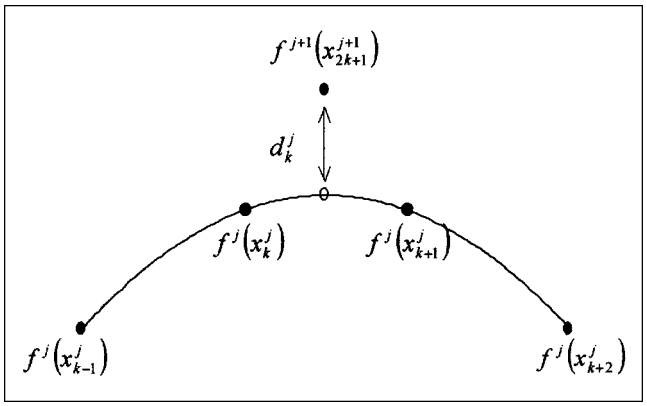

Figure 2. Example of wavelet coefficients calculation (cubic interpolation).

resolution: defining the wavelets in the interval boundaries, grid adaptation, and the calculation of the derivatives in an adapted grid.

Wavelets in interval boundaries

The interpolating wavelets are defined in an infinite domain; however, in the resolution of partial differential equations, the domain is usually finite. To overcome this obstacle, different approaches have been proposed in literature:

(1) Construct a wavelet family in the boundary, different from the one defined inside the interval, which also possesses the interpolating property, following the ideas of Donoho (Donoho, 1992). This approach was used by Bertoluzza (1996) and Cruz et al. (2001)

(2) Construct a generalized wavelet family (Shi et al., 1999)

(3) Define a prolongation operator in the interval boundary (Vasilyev et al., 1995; Vasilyev and Paolucci, 1996).

The definition of a prolongation operator in the interval boundary is the most intuitive solution; however, the extrapolation of the function values outside the interval results in significant errors. The treatment of (Shi et al., 1999) is more versatile than the construction presented by (Donoho, 1992). This versatility will be tested with the problems presented here.

Grid adaptation

In order to illustrate the grid-adaptation algorithm, we shall consider the function $f(x)$, defined in a closed interval $[a,b]$. As discussed, the interpolating wavelets are constructed in the dyadic grid points (Figure 1). The function can be approximated as

$$f^{J\max}(x) = \sum_{k=0}^{2^{J\min}} s_k^{J\min}\phi_k^{J\min} + \sum_{j=J\min}^{J\max-1}\sum_{k=0}^{2^j} d_k^j\psi_k^j \qquad (10)$$

For functions that possess small and isolated scales, most of the wavelet coefficients, d_k^j, calculated through the wavelet transform, are close to zero. A good description of the function can therefore be obtained neglecting a significant number of wavelets associated with such coefficients. Equation 10 can be rewritten as a sum of two terms, each involving the wavelets whose coefficients are larger or smaller than a given threshold

$$f^{J\max}(x) = f_{\geq}^{J\max}(x) + f_{<}^{J\max}(x), \qquad (11)$$

where

$$f_{\geq}^{J\max}(x) = \sum_{k=0}^{2^{J\min}} s_k^{J\min}\phi_k^{J\min} + \sum_{j=J\min}^{J\max-1}\sum_{\substack{k=0\\ |d_k^j|\geq\epsilon}}^{2^j} d_k^j\psi_k^j \qquad (12)$$

and

$$f_{<}^{J\max}(x) = \sum_{j=J\min}^{J\max-1}\sum_{\substack{k=0\\ |d_k^j|\geq\epsilon}}^{2^j} d_k^j\psi_k^j \qquad (13)$$

Donoho (1992) demonstrated that

$$|f^{J\max}(x) - f_{\geq}^{J\max}(x)| \leq C\epsilon \qquad (14)$$

that is, the difference between $f^{J\max}(x)$ and the approximate function $f_{\geq}^{J\max}(x)$ is always lower than a constant, C, times a threshold, ϵ. The value of the constant is finite and depends on the value of $f^{J\max}(x)$ (Donoho, 1992). Therefore, as ϵ tends to zero, the approximation $f_{\geq}^{J\max}(x)$ becomes exact.

As each wavelet ψ_k^j is uniquely associated with one collocation point x_{2k+1}^{j+1}, this should be omitted from the grid whenever the wavelet ψ_k^j is rejected from the approximation $f_{\geq}^{J\max}(x)$. In this procedure it should be guaranteed that: $V_{\geq}^j \subset V^j$ and that $V_{\geq}^j \subset V_{\geq}^{j+1}$, for $J\min \leq j \leq J\max$ in order to satisfy the multiresolution analysis.

This grid-reduction technique was numerically tested with the function

$$f(x) = \exp\left\{-\frac{(x-x_0)^2}{\epsilon}\right\} \qquad (15)$$

and with $x_0 = 0.5$, $\epsilon = 1.0\times10^{-4}$, $J\min = 3$ and $J\max = 15$.

Figure 3a shows the resulting approximate function, $f_{\geq}^{J\max}(x)$, and Figure 3b shows the collocation points location, x_k^j.

In resolution of PDEs, the grid should be continually adapted, so that it can automatically adjust to reflect modifications in the solution. The grid-adaptation strategy adopted here was the following:

(1) Given discrete function values, $f(x_k^j)$ in a grid V^j and at time $t = t_1$, compute the wavelet transform to obtain the values of $s_k^{J\min}$ and d_k^j for $J\min \leq j \leq J\max-1$.

(2) Identify the wavelets coefficients, d_k^j, that fall above the predefined threshold, ϵ. The corresponding grid points, x_{2k+1}^{j+1}, are included in an indicator.

(3) Add points $x_{2(k+1)+1}^{j+1}$, $i = -NL, NR$, to the indicator. These are the collocation points to the right and left of the previous ones, at the same resolution level. This is done in order to account for possible translation of the sharp features of the solution in the next time integration steps.

(4) Add points x_{4k+1}^{j+2} and x_{4k+3}^{j+2} to the indicator. These are the collocation points in the resolution level immediately above. This accounts for the possibility of the solution becoming "steeper" in this region.

(5) Add to the indicator the collocation points associated with the scaling function in the lower resolution level, $J\min$. These are the "basic" grid points, which are always present.

(6) Beginning at resolution level $j = J\max-1$, recursively extend the indicator, so that all the grid points necessary for the calculation of the existing jth-level wavelet coefficients are included.

This strategy was shown to be efficient in the resolution of single-equation problems. For resolution of PDE systems, the previous procedure must be modified to reflect the behavior of the solutions of all equations. This way, the indicator should include information from all the PDEs.

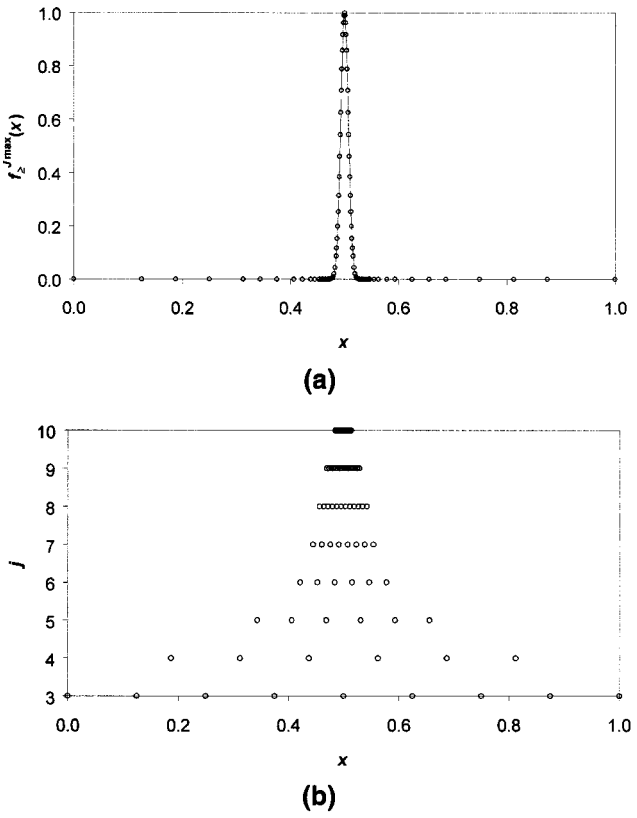

Figure 3. Grid-reduction example using the test function given by Eq. 15.

(a) Function values in the grid points; (b) corresponding distribution of the grid points in terms of spatial location and resolution level. The parameters used in the adaptation algorithm are $\epsilon = 1.0 \times 10^{-4}$ and $m = 4$.

Calculation of space derivatives in adapted grid

When a PDE is solved, it is necessary to compute the function's first and second derivatives in the grid points. Three methods were presented in the open literature for doing this:

(1) Differentiation of Eq. 10 and calculation of the derivatives in the grid points, applying derivative operators (Vasilyev et al., 1996; Vasilyev and Paolucci, 1997).

(2) Evaluation of the derivatives in an irregular grid (Jameson, 1998; Cruz et al., 2001)

(3) Interpolation of the solution to the maximum resolution level and calculation of the derivatives in a uniform grid (Holmstrom, 1999)

Holmstrom's method is not convenient, since the interpolation up to the maximum resolution level is a fastidious process that involves too many unnecessary calculations. The other two methods are much simpler and intuitive. The first is the only one considered to be a pure wavelet resolution method. However, the second method is more versatile, since it only uses the wavelets to determine an optimal grid and then calculates the derivatives by a method of choice, for example, finite differences using Lagrange polynomials, and cubic splines.

The first and the second methods were tested in the resolution of the problems presented here. The second method was shown to be much more efficient and versatile.

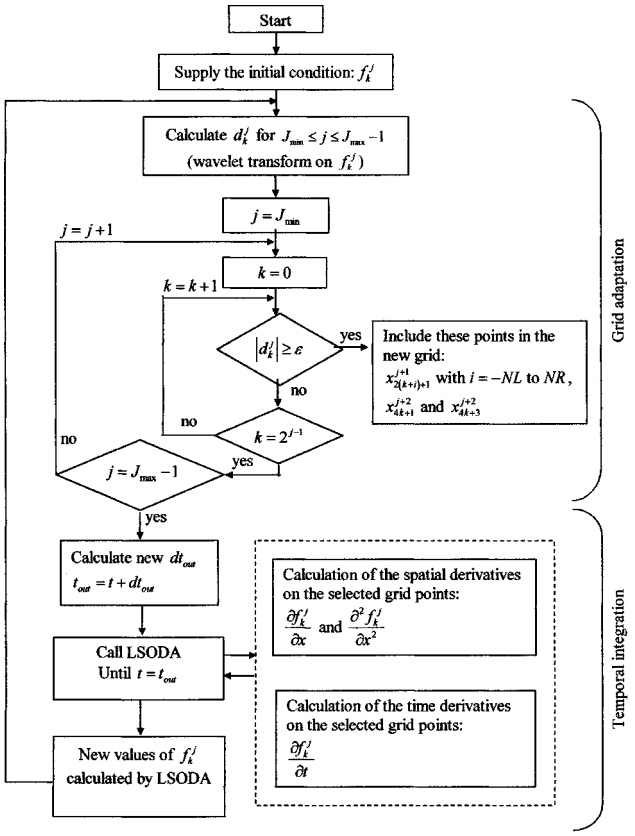

Figure 4. Complete PDE solution algorithm.

Temporal Integration

In this work, the integration of the resulting system of ordinary differential equations (ODEs—initial-value problem), one for each grid point, was done with package LSODA (Petzold and Hindmarsh, 1997). The grid adaptation was performed dynamically throughout the integration. In order to save computation time and avoid superfluous grid adaptations, a criterion was implemented for adjusting the time interval along which the grid stays unchanged, dt_{out}. This is based on the amount of change the grid suffers between two consecutive adaptations and on the progress of the solution (in terms of the magnitude of the time derivatives). This capability is of great importance in the solution of problems where the time scale is unknown *a priori*.

Figure 4 summarizes the complete algorithm, involving the grid adaptation and temporal integration procedures.

Application Examples

The next examples attempt to prove the effectiveness of the method dealing with some of the most common phenomena in chemical engineering: adsorption (fixed-bed multicomponent adsorption model), reaction (nonisothermal catalytic reactor model), and fluid flow (Buckley–Leverett problem, Burger's equation, and Couette flow problem). All the results presented were calculated on a personal computer, Pentium III 700 MHz with 128 M DRAM. Examples 1 and 2 refer to

single-equation problems, while Examples 3, 4 and 5 deal with systems of partial differential equations.

Example 1: Buckley – Leverett problem

The Buckley–Leverett problem results from the application of the material balance equations to two immiscible fluids (water and oil), one being displaced by the other in a porous medium. If the densities of the two phases are considered constant, the system of equations can be substituted by a single equation. This manipulation is based on the fact that the sum of the saturations equals one. The equation that transcribes the problem is (Finlayson, 1992)

$$\frac{\partial S_w^*}{\partial \theta} + \frac{\partial f_w(S_w^*)}{\partial x} = 0 \tag{16}$$

where

$$S_w^* = \frac{S_w - S_{wc}}{1 - S_{or} - S_{wc}},\ \theta = \frac{tq}{\epsilon_b L(1 - S_{or} - S_{wc})},\ x = \frac{z}{L}$$

S_w is the dimensionless water saturation, S_{or} is the residual oil saturation and S_{wc} is the connate water saturation, θ is the dimensionless time variable, t is the time variable, ϵ_b is the porosity, L is the capillary length, q is the total flow per unit of area, x is the dimensionless space coordinate, and z is the space coordinate.

The solution of the problem is presented with f_w given by the following expression (Finlayson, 1992)

$$f_w(S_w^*) = \frac{S_w^*}{S_w^{*3} + \frac{2}{3}(1 - S_w^*)^3} \tag{17}$$

Initial condition: $\theta = 0, S_w^* = 0, \forall x$

Boundary conditions: $x = 0, S_w^* = 1, \forall \theta$

The simulation results are presented in Figure 5. The parameters used in the adaptation algorithm are $\epsilon = 1.0 \times 10^{-3}$, $NR = NL = 2$, and $m = 4$. In this and in all the examples presented next, space derivatives were computed in an irregular grid using cubic splines. The simulation results are presented in Figure 5. Figure 5a shows the spatial variation of S_w^* with x, while Figure 5b shows the distribution of the grid points in terms of space location and resolution level. It is clear that the algorithm has placed the highest concentration of grid points in the region where the profile exhibits a sharp front. The resolution level goes up to 12 in this region. Some points were also placed in the lower x region, where a steep curvature in S_w^* is visible, but the maximum resolution level is only 7 in that region.

For this particular problem, Finlayson (1992) showed that conventional fixed-grid methods fail to obtain the correct solution. Acceptable results were only obtained with a moving-grid collocation method, but this implied using information on the known front velocity. On the other hand, the wavelet-grid adaptation method presented here works in a "self-sufficient" fashion, without demanding such problem-specific information.

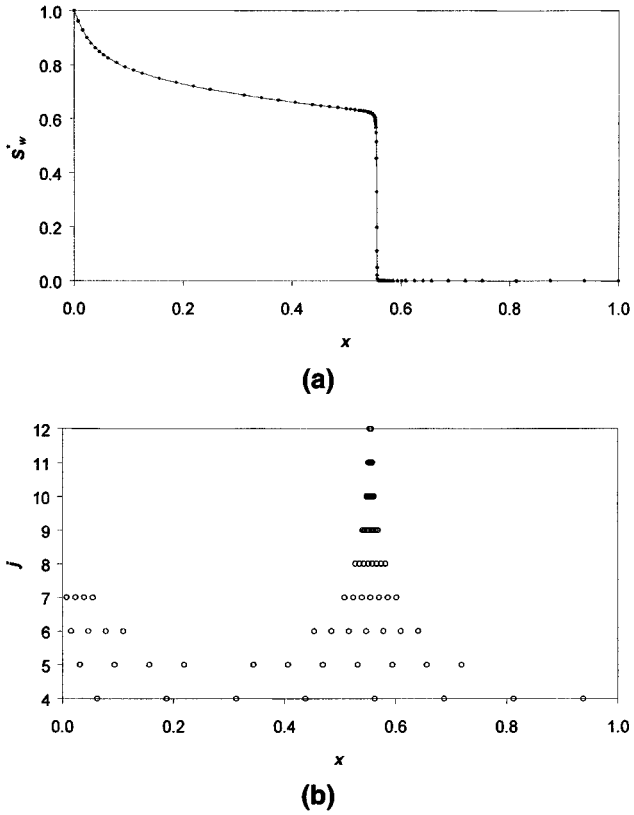

Figure 5. Solution of Buckley–Leverett problem.

(a) Dimensionless water saturation $\theta = 0.4$; (b) corresponding distribution of the grid points in terms of spatial location and resolution level. The parameters used in the adaptation algorithm are $\epsilon = 1.0 \times 10^{-3}$, $NR = NL = 2$, and $m = 4$. Space derivatives were computed in an irregular grid (cubic splines).

Example 2: Burger's equation

Burger's equation results from the application of the Navier–Stokes equation to unidirectional flow without pressure gradient. It is also a problem that arises from Fokker–Planck equation and those governing the spreading of liquids on solids

$$\frac{1}{Re}\frac{\partial^2 u^*}{\partial x^2} = \frac{\partial u^*}{\partial \theta} + u^*\frac{\partial u^*}{\partial x} \tag{18}$$

where u^* is the dimensionless velocity $u^* = u/u_{\text{ref}}$, x is the dimensionless space coordinate $x = z/L$; θ is the dimensionless time variable $\theta = tu_{\text{ref}}/L$; Re is the Reynolds number $Re = Lu_{\text{ref}}/\upsilon$; u_{ref} is the reference velocity; z is the space coordinate; L is the characteristic length; t is the time variable; and υ is the fluid viscosity.

Initial condition: $\theta = 0, u^* = \frac{1}{2}\sin(\pi x) + \sin(2\pi x)$

Boundary conditions: $x = 0,\ u^* = 0,\ x = 1,\ u^* = 0,\ \forall \theta$

The simulation results with $Re = 1.0 \times 10^4$ are presented in Figure 6. The parameters used in the adaptation algorithm are $\epsilon = 1.0 \times 10^{-5}$, $NR = NL = 2$, and $m = 4$. Figure 6a and 6b refer to a dimensionless time, $\theta = 0.1$. A steep change in u^* is starting to develop for x close to 0.6. Therefore, extra grid points are placed around that location, and the resolution level goes up to 8. For a later dimensionless time, $\theta = 1.0$, as seen in Figure 6c and 6d, the change has become an abrupt step and the grid resolution has to go up to the maximum level of 12.

Burger's equation is traditionally used to test the performance of numerical methods. A fixed-grid method (using cubic splines for computing the derivatives) with $2^{11} + 1$ grid points takes about 18 times longer to reach the solution for $\theta = 1.0$, and the result shows oscillations about the exact solution. With a lower number of points ($< 2^{10} + 1$) any fixed-grid method simply fails to carry the integration to the end.

Example 3: fixed-bed multicomponent adsorption model

The model used for describing the fluid-phase mass balances considers axially dispersed plug-flow, constant flow velocity, negligible pressure drop, and isothermal operation. There are *nc* such mass-balance equations

$$\frac{1}{Pe}\frac{\partial^2 c_i^*}{\partial x^2} = \frac{\partial c_i^*}{\partial x} + \frac{\partial c_i^*}{\partial \theta} + \zeta \frac{\partial \bar{q}_i^*}{\partial \theta}, \; i = 1, nc \tag{19}$$

Two models will be considered for the mass-transfer between the fluid phase and the adsorbed phase

Equilibrium model: $\bar{q}_i^* = q_i^*$.

Linear driving-force model: $\dfrac{\partial \bar{q}_i^*}{\partial \theta} = R_i^{bD}(q_i^* - \bar{q}_i^*)$,

with

$$R_i^{bD} = \frac{15 D_i^e L}{R_p^2 u} \; i = 1, nc$$

where *nc* is the number of components; c_i^* is the dimensionless fluid-phase concentration of the i component $c_i^* = c_i/c_{\text{ref}}$; q_i^* is the dimensionless adsorbed-phase concentration of the i component in equilibrium with c_i^* $q_i^* = q_i/q_{\text{ref}}$, $\bar{q}_i^*$ is the dimensionless average adsorbed-phase concentration of the i component; x is the dimensionless space coordinate $x = z/L$; θ is the dimensionless time variable $\theta = tu/L$; Pe is the Peclet number $Pe = Lu/D_{\text{ax}}$; ζ is the bed-capacity factor $\zeta = (1 - \epsilon_b)/\epsilon_b q_{\text{ref}}/c_{\text{ref}}$; u is the flow velocity; z is the space coordi-

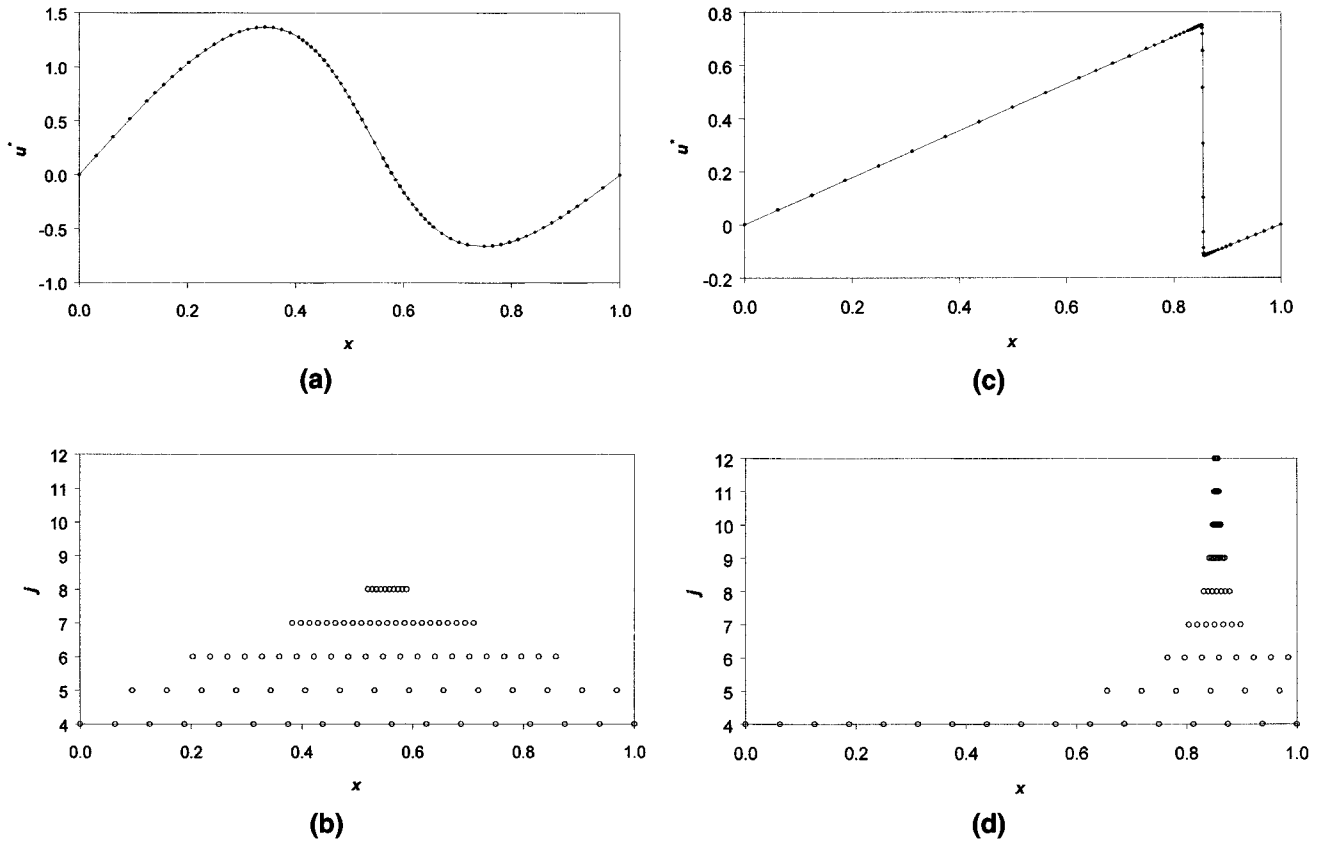

Figure 6. Solution of Burger's equation with $Re = 1.0 \times 10^4$.

(a) Dimensionless velocity as a function of x for $\theta = 0.1$; (b) corresponding distribution of the grid points in terms of spatial location and resolution level; (c) dimensionless velocity as a function of x for $\theta = 1.0$; (d) corresponding distribution of the grid points in terms of spatial location and resolution level. The parameters used in the adaptation algorithm are $\epsilon = 1.0 \times 10^{-5}$, $NR = NL = 2$, and $m = 4$. Space derivatives were computed in an irregular grid (cubic splines).

nate; L is the column length; t is the time variable; D_{ax} is the axial dispersion coefficient; ϵ_b is the bed porosity; q_{ref} is the reference adsorbed phase concentration; and c_{ref} is the reference fluid-phase concentration.

The adsorption isotherm considered is:

$$q_i^* = \frac{R_i^Q c_i^*}{1 + \sum_{i=1}^{nc} R_i^K c_i^*}$$

Initial condition: $\theta = 0$, $c_i^* = 0$, $\forall x$. Boundary conditions:

$$x = 0, \ \frac{1}{Pe}\frac{\partial c_i^*}{\partial x} = c_i^* - c_{i,\text{in}}^*(\theta), \ x = 1, \ \frac{\partial c_i^*}{\partial x} = 0, \ \forall\theta$$

The example was tested numerically for the problem of a moving concentration peak along the column, $c_{i,\text{in}}^*(t) = y_i \delta(t)$, where y_i is the inlet molar fraction

$$\delta(t) = \begin{cases} 1/T & \text{if} \quad 0 \le t \le T \\ 0 & \text{if} \quad t > T \end{cases} \qquad T = 1 \times 10^{-3}$$

The simulation results, with $nc = 2$, $R_1^K = 0.1$, $R_1^Q = 1$, $R_2^K = 0.01$, $R_2^Q = 0.1$, $Pe = 1 \times 10^4$, $\zeta = 1$, and the equilibrium model are presented in Figure 7a and 7b. The results corresponding to the linear driving-force model, with $R_1^{bD} = 100$ and $R_2^{bD} = 100$, are presented in Figure 7c and 7d. The parameters used in the adaptation algorithm are $\epsilon = 1.0 \times 10^{-3}$, $NR = NL = 2$, and $m = 4$. Figure 7b shows how the grid points were selected by the algorithm in order to properly describe the two concentration peaks. It is interesting to note that high resolution levels are used not only at the sharp peak front but also at the tail end, where a change in curvature occurs. This is particularly visible for the concentration peak of component 1, the most strongly adsorbed. The effect of not considering instantaneous equilibrium is shown in Figure 7c and 7d. The higher dispersion effects introduced by the mass-transfer resistance cause a broadening of the peaks, and therefore lower grid resolutions are used.

Example 4: nonisothermal catalytic reactor model

The model presented is a nonisothermal catalytic reactor with a pseudohomogenous first-order exothermic irreversible reaction: $A \rightarrow$ products.

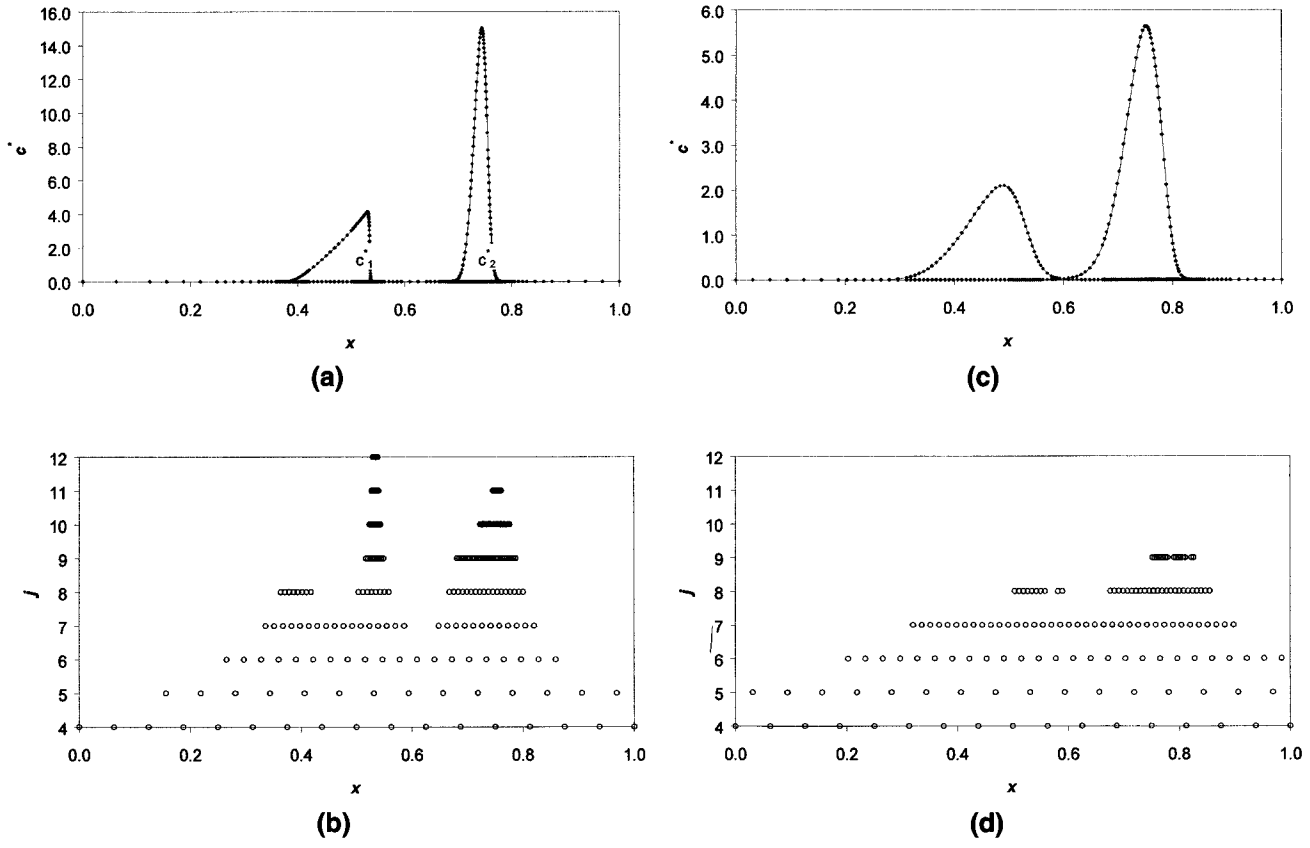

Figure 7. Solution of fixed-bed multicomponent adsorption model.

(a) Dimensionless fluid-phase concentration for equilibrium model with $R_1^K = 0.1$, $R_1^Q = 1$, $R_2^K = 0.01$, $R_2^Q = 0.1$, $Pe = 1.0 \times 10^4$, $\zeta = 1$, and $\theta = 0.8$; (b) corresponding distribution of the grid points in terms of spatial location and resolution level; (c) dimensionless fluid-phase concentration for linear driving force model with, in addition to the previously defined parameters, $R_1^{bD} = 100$ and $R_2^{bD} = 100$; (d) corresponding distribution of the grid points in terms of spatial location and resolution level. The parameters used in the adaptation algorithm are $\epsilon = 1.0 \times 10^{-3}$, $NR = NL = 2$, and $m = 4$. Space derivatives were computed in an irregular grid (cubic splines).

The main model assumptions are: axially dispersed plug-flow, negligible radial gradients, negligible pressure drop, constant interstitial velocity, kinetic constant dependence on temperature according to the van't Hoff equation, thermal equilibrium between the stationary phase and the mobile phases, constant heat capacities, constant densities, and negligible heat accumulation in the column wall. The two problem's equations are

$$\frac{1}{Pe}\frac{\partial^2 c^*}{\partial x^2} = \frac{\partial c^*}{\partial x} + \frac{\partial c^*}{\partial \theta} + Da\, c^* \exp\left\{R^E\left(1-\frac{1}{T^*}\right)\right\} \tag{20}$$

$$\frac{1}{Pe_H}\frac{\partial^2 T^*}{\partial x^2} = \frac{\partial T^*}{\partial x} + R^H\frac{\partial T^*}{\partial \theta} + N_W(T^*-1) - \beta c^* \exp\left\{R^E\left(1-\frac{1}{T^*}\right)\right\} \tag{21}$$

where

$$c^* = c/c_{ref}, \quad T^* = T/T_{\text{ref}}, \; \theta = t/\tau_b, \; \tau_b = L/u, \; Da = \frac{k_{\text{ref}}\tau_b}{\epsilon_b}$$

$$\beta = \frac{(-\Delta H)k_{\text{ref}}\tau_b c_{\text{ref}}}{\epsilon_b T_{\text{ref}}\rho Cp}, \; R^E = -\frac{E}{\Re T_{\text{ref}}}, \; Pe = \frac{Lu}{D_{ax}}$$

$$Pe_H = \frac{Lu_b Cp\rho}{k_{ax}}, \; N_W = \frac{2h\tau_b}{R_b\epsilon_b\rho Cp}$$

$$R^H = \frac{\epsilon_b Cp\rho + (1-\epsilon_b)Cp_s\rho_s}{\epsilon_b Cp\rho}$$

Initial condition: $\theta = 0, \quad c^* = 0, \quad T^* = 1, \quad \forall x$

Boundary conditions:

$$x = 0, \frac{1}{Pe}\frac{\partial c^*}{\partial x} = c^* - 1$$

$$\frac{1}{Pe_H}\frac{\partial T^*}{\partial x} = T^* - 1, \quad \forall\theta$$

$$x = 1, \quad \frac{\partial c^*}{\partial x} = 0 \frac{\partial T^*}{\partial x} = 0, \quad \forall\theta,$$

where c is the fluid-phase concentration, T is the tempera-

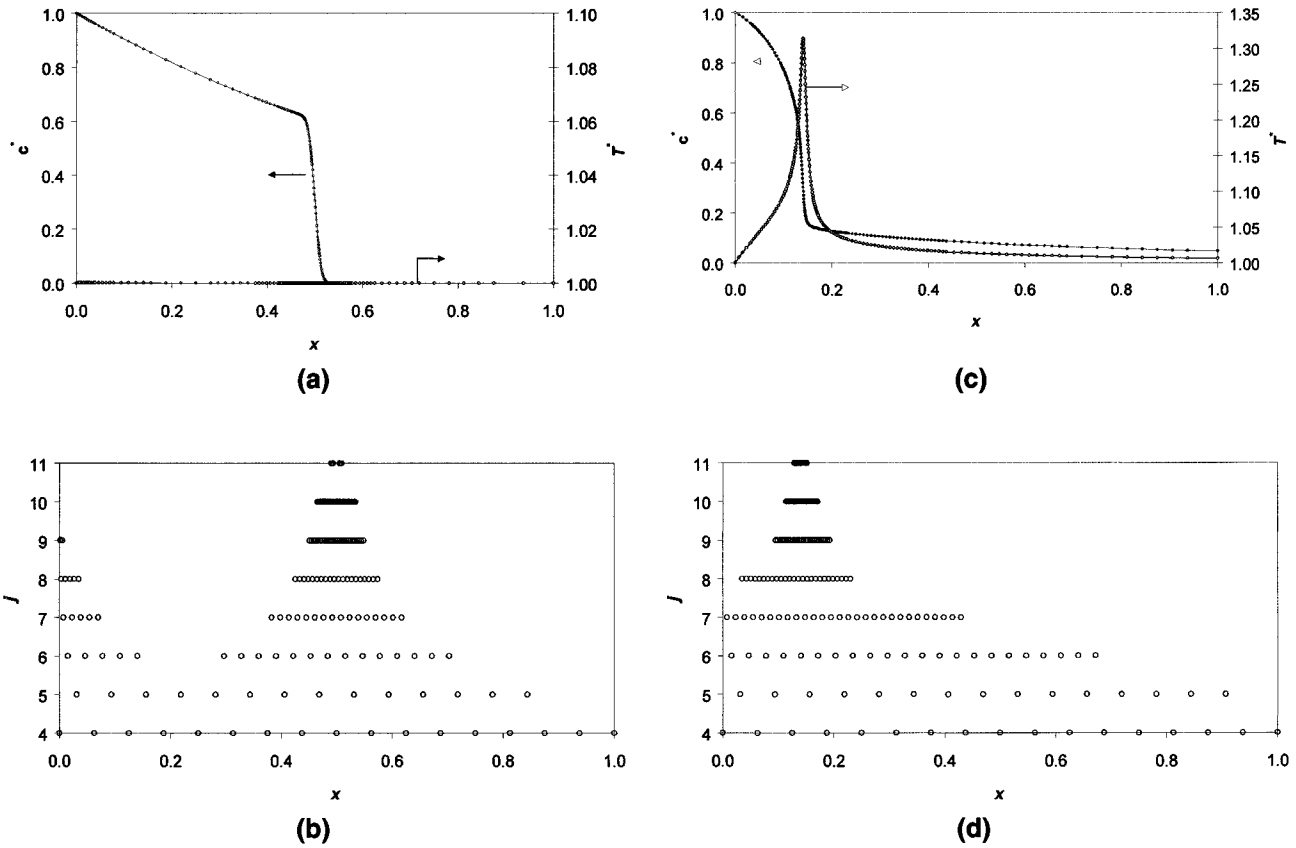

Figure 8. Solution of the nonisothermal catalytic reactor model ($Da = 1$, $\beta = 1$, $R^E = 20$, $R^H = 5{,}000$, $Pe = Pe_H = 1.0 \times 10^4$, and $N_W = 30$).

(a) Dimensionless concentration and temperature profiles for $\theta = 0.5$; (b) corresponding distribution of the grid points in terms of spatial location and resolution level; (c) dimensionless concentration and temperature profiles for $\theta = 750$; (d) corresponding distribution of grid points in terms of spatial location and resolution level. The parameters used in the adaptation algorithm are $\epsilon = 1.0 \times 10^{-5}$, $NR = NL = 2$, and $m = 4$. Space derivatives were computed in an irregular grid (cubic splines).

ture, t is the time variable, L is the column length, u is the velocity, k is the velocity reaction constant, ΔH is the heat of reaction, h is the overall heat-transfer coefficient, R_b is the inner column radius, Cp_s is the solid heat capacity, ρ_s is the solid density, D_{ax} is the axial dispersion coefficient, k_{ax} is the axial thermal conductivity coefficient, z is the axial space coordinate, Cp is the gas heat capacity, ρ is the gas density, ϵ_b is the bed porosity, E is the activation energy, and $\Re$ is the ideal gas constant. The superscript asterisk designates dimensionless variables, and the subscript "ref" means reference.

The simulation results with $Da = 1$, $\beta = 1$, $R^E = 20$, $R^H = 5{,}000$, $Pe = Pe_H = 1.0 \times 10^4$, and $N_W = 30$ are presented in Figure 8. The parameters used in the adaptation algorithm are $\epsilon = 1.0 \times 10^{-5}$, $N_R = N_L = 2$, and $m = 4$. Figure 8a and 8b correspond to a short dimensionless time, $\theta = 0.5$. The reactant's concentration front moves along the reactor, and the temperature still essentially remains unchanged. The grid points are placed where changes in concentration gradient occur. Some extra points are located close to $x = 0$, because the Danckwerts boundary condition imposed for that location causes a small change in gradient in the vicinity of $x = 0$. For a longer time, $\theta = 750$, as seen in Figure 8c and 8d, steady-state operation is approached, and the reactant is rapidly consumed in the initial portion of the reactor, where a temperature "hot-spot" develops. The grid points are placed so that the concentration and temperature changes are properly described.

Example 5: Couette flow problem

This problem considers, for example, a polymer melt held between two plates, initially at rest. A force is applied to the bottom plate, which begins to move at a constant velocity, while the top plate stays in a fixed position. The object of this problem is to calculate the fluid velocity and the stress distribution as a function of time, in the whole domain.

If one assumes that the flow occurs only in the x-direction, and that all the variables depend only on the space variable y, then the momentum balance equation is (Bird et al., 1960)

$$\rho \frac{\partial u}{\partial t} = - \frac{\partial \tau_{xy}}{\partial y} \tag{22}$$

where ρ is the fluid density, u is the velocity, τ_{xy} is the x,y element of the stress tensor, t is the time variable, and y is the axial coordinate. The constitutive equations are

$$\tau_{xy} + \lambda \frac{\partial \tau_{xy}}{\partial t} = - \mu \frac{\partial u}{\partial y} \tag{23}$$

$$\tau_{xx} + \lambda \frac{\partial \tau_{xx}}{\partial t} = 2 \lambda \tau_{xx} \frac{\partial u}{\partial y} \tag{24}$$

$$\tau_{yy} + \lambda \frac{\partial \tau_{yy}}{\partial t} = 0 \tag{25}$$

where λ is a time constant.

The dimensionless equations are

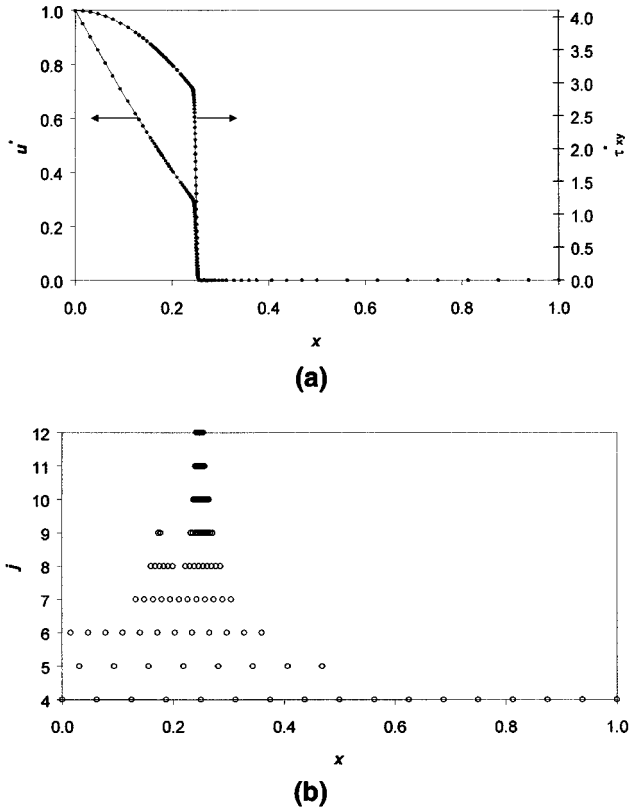

Figure 9. Solution of the Couette flow problem.

(a) Dimensionless velocity and stress for $\theta = 0.025$; (b) distribution of the grid points in terms of spatial location and resolution level. The parameters used in the adaptation algorithm are $\epsilon = 1.0 \times 10^{-3}$, $NR = NL = 2$, and $m = 4$. Space derivatives were computed in an irregular grid (cubic splines).

$$\frac{\partial u^*}{\partial \theta} = - \frac{\partial \tau^*_{xy}}{\partial y^*} \tag{26}$$

$$\tau^*_{xy} + E \frac{\partial \tau^*_{xy}}{\partial \theta} = - \frac{\partial u^*}{\partial y^*} \tag{27}$$

$$\tau^*_{xx} + E \frac{\partial \tau^*_{xx}}{\partial \theta} = 2 We \tau^*_{xy} \frac{\partial u^*}{\partial y^*} \tag{28}$$

where

$$u^* = \frac{u}{u_{ref}},\ \theta = \frac{t\mu}{\rho L^2},\ \tau^*_{xy} = \frac{\tau_{xy} L}{\mu u_{\text{ref}}},\ y^* = \frac{y}{L},\ E = \frac{\lambda \mu}{\rho L^2}$$

and $We = \dfrac{\lambda u_{ref}}{L}$.

Initial condition: $\theta = 0$, $u = 0$, $\forall y^*$.

Boundary conditions: $y^* = 0$, $u^* = 1$; $y^* = 1$, $u^* = 0$, $\forall \theta$.

Equations 26 and 27 should be solved simultaneously, while Eq. 28 can be solved separately. The solution of the system of Eqs. 26 and 27, with $E = 0.01$, is presented in Figure 9a and 9b. The parameters used in the adaptation algorithm are $\epsilon = 1.0 \times 10^{-3}$, $NR = NL = 2$, and $m = 4$.

Conclusions

The grid adaptation method presented here, based on interpolating wavelets, proved to be efficient and accurate in the resolution of PDE problems involving different types of sharp fronts and transitions. A higher density of grid points is automatically allocated to those domain regions where the transient solution exhibits abrupt changes, while a sparse grid is used everywhere else. The maximum and minimum grid resolution levels that are usable by the algorithm are user-defined, avoiding grid coalescence. The implementation of the algorithm is simple, modular, flexible, and problem-independent, without demanding any prior knowledge of the problem's solution. Once the grid adaptation subroutine is available, it can be incorporated into any generic PDE solution package, in conjunction with any appropriate differential operator.

Some of the intended future work in this area deals with the extension of the method to problems involving multiple spatial dimensions.

Acknowledgments

The work of Paulo Cruz was supported by FCT (Grant BD/21483/99).

Notation

c = fluid-phase concentration, mol/dm^3
Cp = fluid-phase heat capacity, J/(K·kg)
Cp_s = solid heat capacity, J/(K·kg)
d = wavelet function coefficient
Da = Damköhler number, $(k_{\text{ref}}\tau_b)/\epsilon_b$
D_{ax} = effective axial dispersion coefficient, m^2/s
dt_{out} = time interval along which the grid stays unchanged, s
E = Couette flow parameter, $\lambda\mu/\rho L^2$
E = activation energy, J/mol
g, h = wavelet filters
$\tilde{g}, \tilde{h}$ = dual wavelet filters
h = overall heat-transfer coefficient, W/(m^2·K)
$J_{\min}$ = minimum resolution level
$J_{\max}$ = maximum resolution level
k = reaction-rate constant, dm^3/(mol·s)
k_{ax} = effective axial thermal conductivity coefficient, J/(m·s·K)
L = column length, m
m = wavelet degree
NL = number of collocation points added to the left
NR = number of collocation points added to the right
N_W = dimensionless parameter, $2h\tau_b/(R_b\epsilon_b\rho C_p)$
Pe = Peclet number, Lu/D_{ax}
Pe_H = thermal Peclet number, $(Lu_bCp\rho)/k_{\text{ax}}$
q = adsorbed phase concentration, mol/dm^3
q = total flow per unit of area, m^3/(m^2·s)
$\Re$ = universal gas constant, J/(mol·K)
R_b = inner column radius, m
R_i^{bD} = dimensionless parameter, $15D_eL/R_p^2u$
Re = Reynolds number, Lu_{ref}/ν
R^E = dimensionless parameter, $-(E/\Re T_{\text{ref}})$
R^H = dimensionless parameter, $[\epsilon_bCp\rho + (1-\epsilon_b)Cp_s\rho_s]/\epsilon_bCp\rho$
R^K = isotherm dimensionless parameter
R^Q = isotherm dimensionless parameter
s = scaling function coefficient
S_{or} = residual oil saturation
S_w = water saturation
S_{wc} = connate water saturation
t = time variable, s
T = dimensionless pulse concentration time
T = temperature, K
t_{out} = final integration time, $t + dt_{\text{out}}$
u = flow velocity, m/s
V = scaling-function space
$\tilde{V}$ = dual scaling-function space
W = wavelet-function space
$\tilde{W}$ = dual wavelet-function space
We = Weinberger number, $\lambda u_{\text{ref}}/L$
x = spatial localization
x = dimensionless spatial coordinate
z = spatiale coordinate

Greek letters

β = dimensionless parameter, $[(-\Delta H)k_{\text{ref}}\tau_bc_{\text{ref}}]/(\epsilon_bT_{\text{ref}}\rho Cp)$
ΔH = heat of adsorption or reaction, J/mol
ϵ = threshold parameter
ϵ_b = bed porosity
ϕ = scaling function
$\tilde{\phi}$ = dual scaling function
ψ = wavelet function
$\tilde{\psi}$ = dual wavelet function
θ = dimensional time variable
ξ = capacity factor, $(1-\epsilon_b)/\epsilon_bq_{\text{ref}}/c_{\text{ref}}$
υ = fluid viscosity, kg/(m·s)
ρ = fluid density, kg/m^3
ρ_s = solid density, kg/m^3
τ_b = bed residence time, (L/u)
τ_{xy} = x-axis component of the stress exerted on a fluid surface of constant y, N/m^2

Superscripts and subscripts

j = resolution level
* = dimensionless variable
in = inlet
k = spatial position
ref = reference
ith = component

Literature Cited

Bacry, E., S. Mallat, and G. Papanicolaou, "A Wavelet Based Space-Time Adaptive Numerical Method for Partial Differential Equations," *RAIRO Model. Math. Anal. Numer.*, **26**, 793 (1992).

Bertoluzza, S., "Adaptive Wavelet Collocation Method for the Solution of Burgers Equation," *Transp. Theory Stat. Phys.*, **25**, 339 (1996).

Bertoluzza, S., "Multiscale Wavelet Methods for Partial Differential Equations," *Wavelets Analysis and Its Applications*, Vol. 6, W. Dahmen, A. Kurdila, and P. Oswald, eds., Academic Press, New York, NY (1997).

Beylkin, G., and J. Keiser, "On the Adaptative Numerical Solution of Nonlinear Partial Differential Equations in Wavelets Bases," *J. Comput. Phys.*, **132**, 233 (1997).

Bird, R., W. Stewart, and E. Lightfoot, *Transport Phenomena*, Wiley, New York (1960).

Cai, W., and J. Z. Wang, "Adaptive Multiresolution Collocation Methods for Initial Boundary Value Problems of Nonlinear PDEs," *J. Numer. Anal.*, **33**, 937 (1996).

Charton, P., and V. Perrier, "A Pseudo-Wavelet Sheme for the Two-Dimensional Navier Stokes Equations," *Mat. Apl. Comput.*, **15**, 139 (1996).

Cruz, P., A. Mendes, and F. D. Magalhães, "Using Wavelets for Solving PDEs: An Adaptive Collocation Method," *Chem. Eng. Sci.*, **56**, 3305 (2001).

Dahmen, W., A. Kunoth, and K. Urban, "A Wavelet Galerkin Method for the Stokes Equations," *Computing*, **56**, 259 (1996).

Daubechies, I., "Orthogonal Bases of Compactly Supported Wavelets," *Commun. Pure Appl. Math.*, **41**, 225 (1988).

Daubechies, I., *Ten Lectures on Wavelets*, SIAM, Philadelphia (1992).

Deslaurier, G., and S. Dubuc, "Symmetric Iterative Interpolation Processess," *Constr. Approx.*, **23**, 1015 (1989).

DeVore, R., and B. Lucier, "Wavelets," *Acta Numerica 92*, A. Iserles, ed., Cambridge Univ. Press, New York (1992).

Donoho, D. L., "Interpolating Wavelet Transforms," Tech. Rep. 408, Dept. of Statistics, Stanford University, Stanford, CA (1992).

Finlayson, B., *Nonlinear Analysis in Chemical Engineering*, McGraw-Hill, New York (1980).
Finlayson, B., *Numerical Methods for Problems with Moving Fronts*, Ravenna Park Publ., Seattle, WA (1992).
Fröhlich, J., and K. Schneider, "An Adaptive Wavelet-Vaguelette Algorithm for the Solution of Nonlinear PDEs," *J. Comput. Phys.*, **130**, 174 (1997).
Graps, A., "An Introduction to Wavelets," *IEEE Comput. Sci. Eng.*, **2**, 50 (1995).
Griebel, M., and F. Koster, "Adaptive Wavelet Solvers for the Unsteady Incompressible Navier-Stokes Equations," Preprint No. 669, Univ. of Bonn, Bonn, Germany (2000).
Holmström, M., "Solving Hyperbolic PDEs Using Interpolating Wavelets," *J. Sci. Comput.*, **21**, 405 (1999).
Holmström, M., and J. Waldén, "Adaptative Wavelet Methods for Hyperbolic PDEs," *J. Sci. Comput.*, **13**, 19 (1998).
Jameson, L., "On the Wavelet Optimized Finite Difference Method," Tech. Rep. 94-9, NASA, Langley Reserch Center, Hampton, VA (1994).
Jameson, L., "A Wavelet-Optimized, Very High Order Adaptive Grid Numerical Method," *J. Sci. Comput.*, **19**, 1980 (1998).
Jawerth, B., and W. Sweldens, "An Overview of Wavelet Based Multiresolution Analyses," *SIAM Rev.*, **36**, 377 (1994).
Kaibara, M. K., and S. M. Gomes, "Fully Adaptive Multiresolution Scheme for Shock Computations," *Godunov Methods: Theory and Applications*, E. F. Toro, ed., Kluwer Academic/Plenum Publishers, Manchester, U.K. (2001).
Lazaar, S., Pj. Ponenti, J. Liandrat, and Ph. Tchamitchian, "Wavelet Algorithms for Numerical Resolution of Partial Differential Equations," *Comput. Methods. Appl. Mech. Eng.*, **116**, 309 (1994).
Liandrat, J., and Ph. Tchamitchian, "Resolution of the 1D Regularized Burguers Equation Using a Spatial Wavelet Approximation," Tech. Rep., NASA Langley Research Center, Hampton, VA (1990).
Mallat, S., "Multiresolution Approximation and Wavelet Orthogonal Bases of $L^2(\mathbb{R})$," *Trans. Amer. Math. Soc.*, **315**, 69 (1989).
Monasse, P., and V. Perrier, "Orthonormal Wavelet Bases Adapted for Partial Differential Equations with Boundary Conditions," *SIAM J. Math. Anal.*, **29**, 1040 (1998).
Petzold, L. R., and A. C. Hindmarsh, LSODA, Computing and Mathematics Research Division, Lawrence Livermore National Laboratory (1997).
Restrepo, J., and G. Leaf, "Wavelet-Galerkin Discretization of Hyperbolic Equations," *J. Comput. Phys.*, **122**, 118 (1995).
Saito, N., and G. Beylkin, "Multiresolution Representations Using the Auto-Correlation Functions of Compactly Supported Wavelets," *IEEE Trans. Signal Processing*, **41**, 3584 (1993).
Sereno, C., *Método Dos Elementos Finitos Móveis— Aplicações Em Engenharia Química*, PhD Thesis, Faculty of Engineering, Univ. of Porto, Porto, Portugal (1989).
Shi, Z., D. J. Kouri, G. W. Wei, and D. K. Hoffman, "Generalized Symmetric Interpolating Wavelets," *Comput. Phys. Commun.,* **119**, 194 (1999).
Strang, G., "Wavelets and Dilation Equations: A Brief Introduction," *SIAM Rev.*, **31**, 613 (1989).
Strang, G., "Wavelets," *Amer. Sci.*, **82**, 250 (1994).
Vasilyev, O. V., S. Paolucci, and M. Sen, "A Multilevel Wavelet Collocation Method for Solving Partial Differential Equations in a Finite Domain," *J. Comput. Phys.*, **120**, 33 (1995).
Vasilyev, O. V., and S. A Paolucci, "Dinamically Adaptative Multilevel Wavelet Colocation Method for Solving Partial Differential Equations in a Finite Domain," *J. Comput. Phys.*, **125**, 498 (1996).
Vasilyev, O. V., and S. Paolucci, "A Fast Adaptive Wavelet Collocation Algorithm for Multidimensional PDEs," *J. Comput. Phys.*, **125**, 16 (1997).
Waldén, J., "Filter Bank Methods for Hyperbolic PDEs," *J. Numer. Anal.*, **36**, 1183 (1999).

Manuscript received May 10, 2001, and revision received Sept. 10, 2001.